



# Online Distributed Relative Positioning Utilizing Multiple Cooperative Autonomous Agents

Nicolas Souli<sup>1</sup> · Panayiotis Kolios<sup>1</sup> · Georgios Ellinas<sup>1</sup>

Received: 8 February 2023 / Accepted: 4 October 2023 / Published online: 2 December 2023  
© The Author(s) 2023

## Abstract

Currently, an unmanned aerial vehicle (UAV) utilizes global navigation satellite systems (GNSS) in conjunction with other modalities for localization purposes. Nevertheless, this approach faces robustness issues when GNSS signals become unavailable or sensors malfunction. Clearly, the robustness of the system increases considerably when multiple UAV agents are employed to perform collaborative positioning. In this work, an online distributed solution is proposed for relative localization, which incorporates multiple UAVs together with Signals of Opportunity (SOPs) as well as inertial, visual, and optical flow measurements. The proposed localization system includes relative self-localization of each UAV agent, as well as a reliable distributed relative positioning system (DRPS) for each UAV based on the relative positions from other UAV agents in its vicinity. The latter positioning strategy is required in case the relative self-localization fails, mainly due to such problems as inertial measurement unit (IMU) accumulated error drift, camera sensor errors, or SOP shortfalls due to multipath or antenna obstruction. Extensive field experiments validate the proposed technique and demonstrate increased localization accuracy and robustness when compared to the benchmark approach that does not include cooperation between UAVs.

**Keywords** Unmanned autonomous vehicles · Signals of opportunity · Cooperative agents

## 1 Introduction

Reliability and precision in location measurements are primary requirements in autonomous vehicle navigation [1]. To date, numerous approaches have been devised to achieve reliable and precise localization, mainly by employing a fusion of various sensor modalities such as visual, inertial, signal processing techniques from satellites (i.e., GNSS) and signals of opportunity (SOPs) [1–5]. The individual localization approaches vary fundamentally in the kinematic models utilized and the filtering techniques employed to estimate the autonomous vehicle's position by compensating for the noise associated with the measurements and reducing the uncertainty in interpreting the sensor signals. The shortfalls of

the various positioning techniques include degradation of the data, signal loss because of multipath or antenna obstruction effects, and signal unreliability, and have led to the investigation of localization methods that exhibit increased robustness [6–13].

With significant advancements in software-defined radios (SDRs), it was not long before SOP-based localization approaches, such as the ones presented in [1, 2, 13, 14], could produce accurate positioning results. The most important benefit of SOP-based solutions is that localization can be achieved when traditional GNSS signals are unavailable due to obstruction from deep urban canyons [11] and due to wireless interference effects [3, 15]. SOPs (usually comprised of TV, radio, and cellular signals) are employed predominantly when the receiver's reference position and the SOP transmitter's location are known a priori. In addition, a fusion of SOP information with other modalities, such as inertial and visual measurements, have been employed to enhance localization [13, 16–18]. Combining various sensor information presents several additional advantages compared to traditional GNSS, including higher accuracy.

Moreover, in addition to sensor fusion onboard individual agents, other research works have looked at multi-agent

✉ Nicolas Souli  
nsouli02@ucy.ac.cy  
Panayiotis Kolios  
pkolios@ucy.ac.cy  
Georgios Ellinas  
gellinas@ucy.ac.cy

<sup>1</sup> KIOS Research and Innovation Center of Excellence and the Department of Electrical and Computer Engineering, University of Cyprus, Nicosia 1678, Cyprus

fusion algorithms to address not only individual sensor faults but also abnormal behavior at the system level. Evidently, the advantages stemming from the distributed schema for the exchange and processing of sensor information among multiple UAVs provide significant gains, especially when heterogeneous agents are considered that use different sensors for self-localization. For instance, the works in [19–22] investigate agent collaboration to address the challenging problem of fusing information originating from many independent and interdependent agents. In those works, it is shown that data fusion can address noise and unreliability of individual sensing modalities. Further, as indicated in [19, 23], it is shown that considering collaboration between multiple agents that provide independent measurement sets can provide robustness in improved localization accuracy.

Overall, a broad body of literature exists on different localization techniques (in terms of single- and multi-agent localization); however, only relatively few have focused on developing efficient online localization algorithms in GNSS-deprived scenarios. This is precisely the focus of this work, which introduces a novel framework for the use of SOPs and other sensor modalities (such as visual and IMU) for online distributed relative positioning between a number of collaborating agents, and details the development and implementation aspects to achieve this in practice. Notably, this work extends our previous single-agent framework detailed in [24, 25] by considering a multi-agent distributed localization framework to realize a robust online relative positioning scheme. In addition to the new modeling framework, this work details the implementation aspects of the proposed approach and validates its feasibility with numerous field experiments.

This work presents two main contributions. First, a novel online multi-agent Distributed Relative Positioning System (DRPS) is introduced, which is capable of localizing a target UAV agent by fusing its relative position information (SOP data, inertial measurements, and optical flow data) along with vision measurements and relative position information from other autonomous agents in the vicinity. Importantly, the proposed system operates without the need for knowing the SOP transmitters' locations or relying on any GNSS signal information. Further, a prototype of the proposed DRPS system is implemented in both hardware and software. Extensive experimental evaluation is conducted in a real-world outdoor environment to demonstrate the system's feasibility. The thorough experimental assessment confirms that the proposed DRPS technique can be effectively applied online, providing precise and accurate UAV relative localization. In summary, the main contributions of this work are as follows: (i) The development of an innovative online multi-agent DRPS, enabling UAV localization through the fusion of various sensor data and relative position information from neighboring agents, all without reliance on SOP transmitter

locations or GNSS signals. (ii) The successful implementation of a prototype DRPS system, combining hardware and software components, and subjected to comprehensive real-world outdoor experiments to showcase its practical viability. The experimental evaluations affirm the system's capability to achieve online and accurate UAV localization.

The proposed solution can be employed as an alternative to GPS-assisted localization, and can be used to maintain navigation perception in cases where the GNSS signals are unavailable or the agent suffers from sensor malfunctions, receiving erroneous data (e.g., inertial navigation system (INS), SOP, visual, or optical flow (OF) data). In particular, results over 70 outdoor experiments illustrate that robust relative positioning can be achieved by incorporating the fused information from the system's agents, achieving a 2-norm error lower than 8 m at 90% of the time compared to single-agent systems.

The rest of the paper is organized as follows. Section 2 outlines the state of the art concerning relative localization, stating how the proposed distributed relative positioning system differs from existing solutions. In Section 3, the DRPS system model is described and the system's architecture is delineated. Sections 4 and 5 describe the local and global frame position estimate subsystems, including the relative frame fusion methodology employed to achieve distributed localization between the collaborating agents. Section 6 presents the algorithmic implementation of the initially-decoupled relative positioning system (RPS) system, and the overall DRPS system that fuses all sensor information collected by the collaborating agents to achieve robust relative positioning. Section 7 includes an extensive performance evaluation of the proposed system, while Section 8 summarizes the key findings and documents avenues of future research work.

## 2 Related Work

### 2.1 SOP-based Techniques

In the literature, numerous approaches utilize SOPs in GNSS-challenged areas. For example, in [1], a ground vehicle navigation approach was employed in areas where GNSS signals were unreliable, that incorporated SOPs in a closed-loop map-matching method. The proposed algorithm used a particle filter to estimate the state of the ground vehicles, assuming a priori knowledge related to the positions of SOP transmitters, and the experimental results demonstrated a root mean square error (RMSE) reduction compared to long-term evolution (LTE)-only localization solution. Also, in [2], SOPs from fixed stations, with known location information, and from mobile GPS-equipped nodes were jointly exploited to cooperatively localize a receiver node by employing a

weighted least squares (WLS) estimator. Furthermore, in [6] SOPs were used to reduce the IMU error variance in the absence of GPS signals. A low complexity semi-definite relaxation algorithm was examined, and simulation results on the Cramér-Rao lower bound demonstrated convergence under specific geometrical and noise limitations. Additionally, the survey in [11] investigated UAV navigation using SOPs in urban environments, discussing various SOP-based positioning techniques that utilized angle of arrival (AoA), time of arrival (ToA), received signal strength (RSS), and time difference of arrival (TDOA). Moreover, in [15], the use of RF signals (such as pseudolites and SOPs) was described for navigation purposes, detailing the opportunities and challenges of navigation when SOPs were employed. Also, in [13], a distributed inertial measurement and SOPs-aided navigation framework was presented, studying vehicle communication in an environment with an imperfect communication channel. Pseudorange observations from unknown SOPs in the vicinity were fused with inertial measurements to obtain navigation with intermittent communication. In a similar vein, the work in [3] proposed an event-based communication strategy for collaborative navigation with SOPs. In that work, it was shown that a team of vehicles obtaining pseudorange measurements from terrestrial SOPs could collaboratively estimate the state of the vehicles and the state of the SOPs, while reducing the amount of data exchanged.

## 2.2 Sensor Fusion Methods

Numerous techniques fuse optical flow, vision, or inertial data to improve the relative positioning procedures. As an example, the work in [5] integrated information extracted by inertial sensors, GPS, and a camera system to compute the altitude and position estimates of a UAV. As the inertial sensors suffer over long-term localization horizons due to drift, GNSS and vision data were coupled to obtain higher accuracy. The proposed system could be used in urban areas, providing position and altitude estimates, but with a lower data rate compared to the inertial sensor measurements. Further, a sensor data fusion ultra-wideband (UWB)-supported inertial navigation method for indoor positioning was considered in [16]. The IMU and UWB modules were attached to a moving person, while data was received by fixed infrastructure nodes. The TDOA technique was followed, along with the IMU information to obtain accurate indoor localization. Further, [17] presented an algorithm for avoiding collisions with walls, that employed optical flow data obtained by a camera mounted on autonomous micro air vehicles (MAVs). To maneuver safely indoors and avoid collisions with walls, a combination of data from IMU and optical flow was utilized that minimized rotational effects. In a similar vein, [18] proposed an extended Kalman filter (EKF)-based scheme that combined optical flow and inertial measurements in order

to avoid navigation system drift and minimize positioning errors in MAVs, thus improving the accuracy of position estimate. Further, in [26], a simultaneous location and mapping (SLAM) methodology was developed on mobile robots, using LiDAR and RGB-D camera information to achieve reliable indoor localization. Finally, in [27], IMU and camera information fusion were employed to improve robustness and localization accuracy. In order to realize greater localization performance, a deep learning-based optical flow approach was utilized and tested on real-world data obtained using low-end computing equipment in a low-texture environment.

## 2.3 Collaborative Localization Techniques

The work in [19] proposed a centralized collaborative monocular architecture, where the data collected were processed at a ground central server (performing map fusion) and fused information was distributed back to the agents, as the agents themselves did not have sufficient computing resources for significant onboard processing. Subsequently, the distributed data were incorporated into the agent's SLAM online estimate. In terms of localization, local map acquisition of the agent's surroundings and pose estimation extraction were performed utilizing visual odometry. This method was limited by the computation capacities of the onboard units and the architecture's significant dependence on the visual dataset, with the system performing better in environments where the accumulated size of the information was manageable. Further, the work in [20] also presented a collaborative pose estimation method between UAV agents that were equipped with inertial sensors and a monocular camera. To compute relative pose estimation, the UAV fields that overlap were extracted by fusing vision-odometry data in an EKF.

Furthermore, the fusion of UWB/LiDAR information for a cooperative range-only SLAM method was presented in [28], within which a mobile robot was employed equipped with a UWB node and a 2D LiDAR sensor and UWB beacons were placed at unknown locations, forming a cooperative sensor network that could extract node range information. Simultaneous localization of the agent was performed, fusing all the UWB nodes and LiDAR mapping data, demonstrating that the UWB range information could improve the LiDAR-based SLAM method. A similar realization was described in [21], where it was shown that the IMU could estimate the changes in position over short-time periods, but in the long term, it was prone to accumulated error. Thus, a UWB ranging unit was applied to mitigate the IMU error (i.e., IMU and UWB range information were fused to attain a cooperative position estimation); however, bearing information was not available and the receiver's location could not be derived. Hence, a particle filter methodology was followed to derive precise position estimates. In [29], UWB anchors were applied on UAVs and along with real-time kinematic

(RTK)-GPS information, precise localization was obtained, while in [30] a UWB-based system was proposed for UAV localization in GNSS-denied environments. However, in both works the UWB range limitation (limiting the reach of the information to a few meters) could lead to a degradation in localization performance.

Moreover, the authors in [23] demonstrated that autonomous UAV agents could exchange information to extract a globally consistent map, employing a vision-based perception (monocular-inertial odometry). The proposed method was evaluated using UAV benchmark datasets, showing a 50% improvement in terms of accuracy as compared to the case where no information was exchanged. Nevertheless, reported fluctuations due to difficult conditions, such as low-texture scenes or bad illumination, emphasized the need for system improvement. In another effort to achieve collaborative localization, the authors in [22] considered a distributed stereo-vision technique in a fleet of MAVs, with sensor data collected from IMU, cameras, and sonar devices incorporated in an EKF to estimate the positions and orientations of all MAVs. This system controlled the formation of the agents in order to maximize their overlapping fields of view. Experiments conducted in indoor environments, with the proposed algorithm applied in a real-time scenario, showed that the collaborative scheme could produce promising results in terms of localization in GPS-denied environments. However, the use of vision data could be a shortfall for the collaborative algorithm in outdoor

environments, as the features extracted from each agent differed only marginally. Finally, in another research effort, the work in [31] demonstrated a distributed algorithm for joint localization, where a team of indoor mobile robots, each equipped with heterogeneous sensors, shared information to compute a combined estimate of the robot poses. The proposed formulation employed a fusion of odometry, IMU, and GPS data, and the pose estimates obtained could be comparable to an EKF design; however, for long-term linear approximations, efficient mechanisms for revising linearizations of process and observation models must be investigated.

In comparison to previous research approaches detailed above, this work introduces a robust online distributed relative positioning technique to obtain the relative trajectory of each agent (e.g., UAV) in a multi-agent system. This is achieved through the employment of a fusion of information obtained from a variety of sensor modalities, including SOPs, IMU, optical flow, and vision data, provided by the UAV agent and other agents in its vicinity that communicate the relevant information to the agent under localization. Such a distributed technique, that combines all these modalities together, implemented in a prototype, and extensively assessed in numerous outdoor field experiments has not been previously presented in the literature.

Figure 1 illustrates a classification of the various more widely-used positioning techniques, and how the proposed technique fits within this classification.

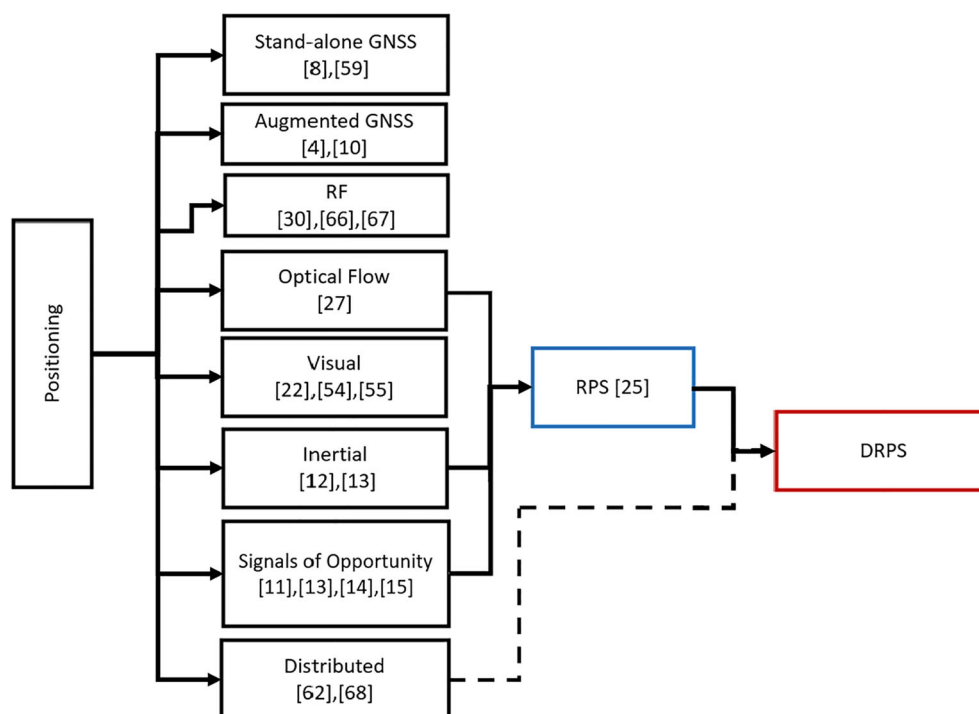


**Fig. 1** Taxonomy of positioning techniques



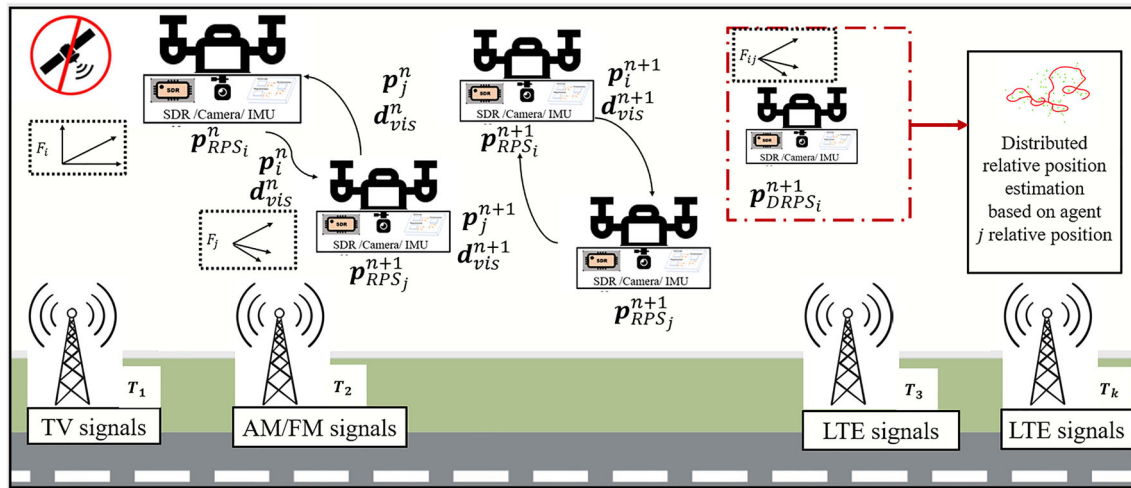


Fig. 2 System model

### 3 System Model

The proposed system model, as shown in Fig. 2, assumes a multi-agent scheme where a number of agents navigate in a 3D space and employ different sensor modalities to accomplish distributed relative positioning. Each agent self-localizes without the use of GNSS information, as software-defined radio (SDR) receivers are utilized to gather SOPs, and at the same time, inertial, visual, and optical flow measurements are collected using an onboard unit. Further, each agent  $i$  employs communication circuitry (i.e., wireless antenna modules available at each agent), so as to exchange information with the rest of the agents in its vicinity (belonging to set  $J$ ) at each time step  $n$ . Specifically, the kinematic principle of any agent  $i$  follows a nonlinear model, and the relative positions of all agents in  $J$  are fused and exchanged in order to extract agent  $i$ 's location based on the information collected from the rest of the agents, as a means to improve accuracy and increase robustness.

Further, while the proposed system does not impose any restrictions on the agents' movements, the following assumptions are made: (i) GNSS is unavailable, (ii) a synchronous system is considered, (iii) agent  $i$  can detect and exchange information with any other agent  $j \in J$ , (iv) the agents are following a predefined path, and (v) the relative position estimation of each agent can be unreliable (due to sensor malfunctions); thus, although a stable relative self-positioning estimation is not assumed, each agent  $i$  can communicate and exchange information with any other agent  $j \in J$  to achieve accurate relative positioning in a distributed manner.

Specifically, in the proposed system model a number of autonomous agents travel in an area where a number of SOP transmitters ( $T_k, k \in \mathcal{K}$ ) are present and onboard each agent there exists a camera, SDR, and IMU. Initially, the trans-

mitter locations  $\mathbf{p}_{T_k}$  are unknown, but subsequently, each agent collects RSS measurements and employs a non-linear least squares (LSQ) method to estimate the transmitter positions (assuming that in the initialization procedure (i.e., the take-off phase), the autonomous agents are able to secure a GNSS fix). When the autonomous agents' GNSS information becomes unreliable or is not available, the relative trajectory of each agent is computed using the RPS methodology by employing the locations of the SOP transmitters ( $\mathbf{p}_{T_k}$ ) and fusing various sensor measurement (e.g., IMU and camera readings) [25, 32]. Specifically, each agent self-localizes by employing a local relative frame  $\mathcal{F}$ , i.e., assuming that an agent  $i$  navigates in an urban area and estimates its location using SOPs, IMU, and vision data modalities (the RPS procedure), a local relative frame  $\mathcal{F}_i$  is generated and maintained in a local reference system (utilizing the agent's initial takeoff position as the initial position). The same pattern is followed for a group of agents in set  $J$  (i.e., in the vicinity of agent  $i$ ), leading to a number of local frames  $\mathcal{F}_j, j \in J$ . The autonomous agents are capable of relative self-localization; however, in cases where some of the sensors utilized for RPS malfunction, and in order to avoid navigation errors and increase robustness, the relative positions of all agents  $j \in J$  in the vicinity of agent  $i$  are employed for distributed relative localization of agent  $i$  (DRPS procedure).

Specifically, the local frame of an agent  $j$ ,  $\mathcal{F}_j$ , along with a range measurement  $\mathbf{d}_c$  (i.e., Euclidean distance between agents  $i$  and  $j$ ), computed using a detection and tracking algorithm, are fused with agent  $i$ 's local frame  $\mathcal{F}_i$  to provide a global relative frame  $\mathcal{F}_{ij}$ , creating a unified relative map using the same reference position. Clearly, this global relative frame will be updated based on which agent  $j$  will be closest to agent  $i$  at each time step. It should be noted that all computational processes, such as the collection of SOPs,

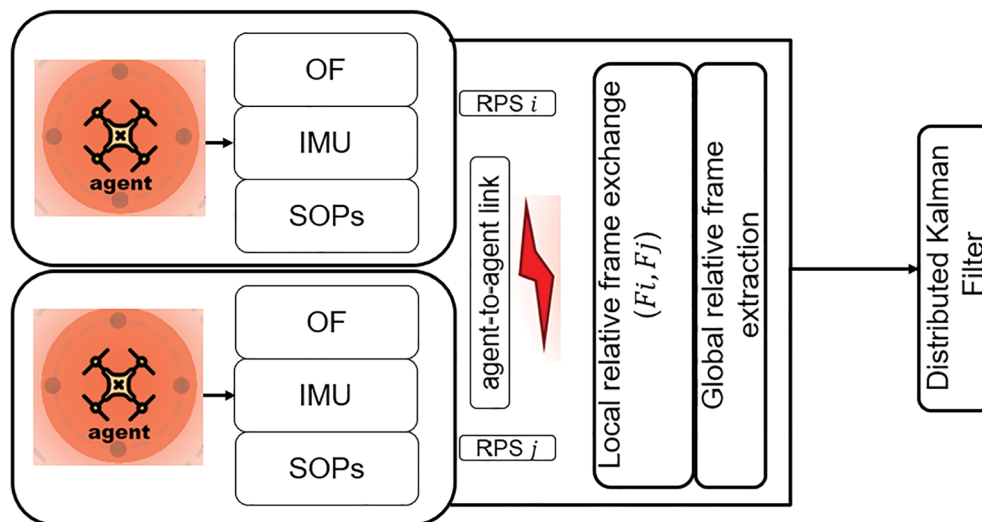


**Fig. 3** DRPS system architecture overview

optical flow, vision detection, frame fusion, and distributed relative position extraction are executed online on an embedded onboard processing unit. The framework design of the proposed DRPS technique is described in Fig. 3. Note that this distributed design does not assume any a priori information on the initial absolute position of the agents. Each agent operates in its local relative position frame and has its current starting position as the initial location.

In terms of information exchanged between the agents, for every time-step  $n$ , all the relative position (RPS) and distance (vision) data, received since the last communication, are disseminated to all agents (i.e., agent  $i$  and all agents in  $J$ ), leading to the combination of distance/vision data that do not belong to the same frame, in order to construct a global relative frame and achieve distributed localization.

This communication is bidirectional, as each agent is able to exchange relative position information with the rest of the agents in its vicinity utilizing an onboard communications module.

## 4 Local Frame Position Estimation

This section summarizes the RPS process employed by each autonomous agent for self-localization when GNSS signals are not available. For a detailed description of the RPS technique, the reader is referred to our previous work in [25, 32]. Subsequently, Section 5 details how enhancements in location accuracy can be achieved through the use of information from surrounding agents.

### 4.1 Modeling the SOPs

Fixed transmitters  $T_k$ ,  $k \in \mathcal{K}$ , with a state vector  $x_{T_k}$  and planar state  $\mathbf{p}_{T_k} = [p_{T_k}(1) \ p_{T_k}(2)]^T$  are following a discrete

model  $\mathbf{p}_{T_k}^{n+1} = \mathbf{F}p_{T_k}^n + \mathbf{w}$  and are used as sources of SOPs (with  $\mathbf{F}$  designating the system dynamics and  $\mathbf{w}$  the process noise). In the RPS framework, the locations of the  $T_k$  relative transmitters are used to compute the trajectory of the autonomous agent by employing the RSS of the SOPs over a number of transmission frequencies [25].

#### 4.1.1 Frequency Band Selection

In SOP-based systems, relative positioning can be established by processing only a subset of the wireless spectrum frequency bands, in order to limit the computational requirements; thus a major challenge in the use of SOPs is frequency ranking and selection [33, 34].

As explained in [33, 35], optimal learning (OL) can be applied to tackle the data gathering and computational load shortcomings. This method relies on statistical parameters to derive the true values of observations, employing the  $\mu^{n+1}$  as the posterior estimate mean with prior mean  $\mu^0$ , covariance  $\Sigma^0$ , and variance  $\lambda$ . The study in [34] describes the knowledge gradient (KG) policy and how it can be utilized to extract measurement decisions online, leading to significant computational cost reductions. Further, our previous work in [36], describes a KG-based frequency selection algorithm (FSA) for the relative positioning system (RPS) that uses correlations in the Bayesian prior beliefs of the frequency band values to enable fast positioning.

### 4.2 Modeling the Agent's Dynamics

The autonomous agent's position ( $\mathbf{p}_{R_i}$ ) and velocity are based on a conventional dynamic model, with agent  $i$  having a planar position  $\mathbf{p}_{R_i}^n = [p_{R_i}(1) \ p_{R_i}(2)]^T$  at time  $n$  and discrete dynamics at sampling time  $n + 1$  given by



To extract the optical flow-based range  $\mathbf{d}_{of}$  and displacement measurements  $[dx_{of}, dy_{of}]$ , a dense optical flow algorithm is applied that utilizes each video frame captured by the onboard camera. In particular, the Farneback OF algorithm is employed [51] that can measure the next pixel position between the two given frames in a pre-defined region of interest (ROI), mainly due to its accuracy in online applications (using the OpenCV library [52]).

Specifically, within the proposed RPS framework, the optical flow technique is employed as follows. At first, the video frame information is gathered online and a grayscale conversion is applied to each frame, which is subsequently employed as input information to the Farneback OF algorithm. This algorithm, at each time-step  $n$ , uses as a reference point the initial video frame and compares it with the video frames that follow. This is done for computing  $(\mathbf{x}_{pixel}, \mathbf{y}_{pixel})$  (i.e., the pixel displacement vectors), as well as the frame's pixels' displacement mean value. In the next step, a meter conversion is implemented employing the ground sample distance (GSD), which expresses the distance between each pixel's center point following a reference ground point and representing each sample on the 2D plane in real size (i.e., in meters) [53]. The agent's altitude, the height, and width of the camera, as well as the camera's focal length and the image's (video stream) width and height are used as input for the GSD computation (with some of these data available through the manufacturer's specifications). Finally, the range measurement  $\mathbf{d}_{of}$  (i.e., the average Euclidean distance over consecutive frames), is computed utilizing the worst-case GSD scenario, as follows:

$$GSD_h = \frac{(D_{of})(B_{of})}{(A_{of})(E_{of})}, \quad GSD_w = \frac{(D_{of})(C_{of})}{(A_{of})(F_{of})}, \quad (1)$$

$$GSD_{final} = \frac{GSD_{worst}}{100}, \quad (2)$$

$$\mathbf{d}_{of} = \sqrt{(|\mathbf{x}_{pixel}|GSD_{final})^2 + (|\mathbf{y}_{pixel}|GSD_{final})^2}, \quad (3)$$

where  $A_{of}$  denotes the focal length,  $B_{of}$  and  $C_{of}$  the height and width of the camera, respectively,  $D_{of}$  the height of the drone, and  $E_{of}$  and  $F_{of}$  the height and width of the image, respectively.

As emphasized above, apart from the range measurement, the displacement of the autonomous agent from the center of the frame must be also computed in order to determine the OF-based position estimate. This displacement can be calculated as  $dis = \frac{X_{of} w_{RP} w_{FP} w_{RP}}{w_{RM} 2w_{RM}}$ , with  $X_{of}$  denoting the center of frame,  $w_{RM}$  and  $w_{RP}$  denoting the reference object's width, in meters and pixels, respectively. Also, the parameters  $w_{Fm}$  and  $w_{FP}$  denote the video frame's width in meters and pixels, respectively, with  $w_{Fm} = \frac{w_{FP} w_{RP}}{w_{RM}}$ .

## 5 Global Frame Position Estimation

In this section, initially, a detailed description of the detection and tracking modules is provided, followed by the fusion of relative frames, for obtaining the global frame position estimate.

### 5.1 Detection and Tracking

In an effort to derive vision-based range and  $X - Y$  coordinates displacement measurements between agents, a drone detection algorithm is utilized. For the detection, an onboard unit is employed to capture video frames using the camera of each agent, while a convolutional neural network, Tiny YOLOv4 [54], is used to detect the collaborating agent (the choice of Tiny YOLOv4 is based on its established performance and accuracy in online applications).

Footage from a UAV flying in close proximity to another agent is acquired and applied as a training dataset that resulted in approximately 10,000 labeled images.

Moreover, a tracking algorithm is used to retain each agent's trajectory over time. In particular, tracking is accomplished using a conventional intersection-of-union scores method and the Hungarian algorithm as described in [55]. When a detection bounding box is achieved, the coordinates are normalized considering the size of the video stream. Then, the detection box area is compared in successive frames and a decision is taken concerning the position of agent  $i$  (pursuer) in relation to agent  $j$  (target) (i.e., agent  $i$ 's flight controller's yaw and throttle signals are provided based on the detected box position and the current posture of agent  $i$ ). Specifically, (i) when the area is larger than 10% of the image, agent  $i$  falls back, as it is considered that it is in very close proximity to agent  $j$ ; (ii) when the area is smaller than 6% of the image, then agent  $i$  moves closer to agent  $j$ , as it is considered to be far from agent  $j$ . At the point where the pursuer drone approaches the target at a certain distance, the data-exchange procedure between the UAVs commences. In this work, data-exchange starts when the detected bounding box is within 7 – 10% of the captured image.

Note that the distance between the agents is computed using the focal length of the camera,  $\mathbf{f} = \frac{w_{RP} d_r}{w_{RM}}$ , acquired at a reference distance  $d_r$ . Specifically, the focal length is used to compute the Euclidean distance as  $\mathbf{d}_c = \frac{w_{RM} \mathbf{f}}{w_{RP}}$  (the assumption in this work is that all agents have similar dimensions).

This detection-and-tracking procedure detects all agents  $j \in J$  that are in range and can communicate with autonomous agent  $i$ . Subsequently, it chooses agent  $j$  that is the closest to agent  $i$ , by employing the Euclidean distance extracted from the vision data, in order to fuse its information with the information of agent  $i$  and obtain the global relative frame.



### 5.2 Fusion of Relative Frames

The fusion module utilizes the relative frames  $\mathcal{F}_i$  and  $\mathcal{F}_j$  of agents  $i$  and  $j$ , respectively. The distance between the two relative frames is computed using the camera (vision data) as previously discussed, and the global initial point is computed in reference to the relative position of agent  $i$ . Thereafter, the two relative frames are combined and a global relative frame  $\mathcal{F}_{ij}$  is derived. Note that a new global relative frame will be computed at some point in the future (i.e., the previous  $\mathcal{F}_{ij}$  will be updated) due to the movement of the agents in set  $J$ , that are employed to extract the distributed relative position.

### 6 DRPS Algorithm

This section describes in detail the implementation of the proposed DRPS algorithm (Algorithm 1), delineating, without loss of generality, the procedure for two autonomous agents. The distributed relative positioning is divided into two phases, the propagation phase, where the information is related to each agent’s relative self-localization (RPS), and the update phase, where the relative position of agent  $j \in J$  is employed to substitute agent’s  $i$  erroneous relative position (e.g., caused due to erroneous sensor measurements).

At first, the relative self-localization of each agent is computed using the various sensor modalities previously explained, followed by the distributed relative positioning process. For simplicity, hereafter, the relative position of agent  $i$  ( $j$ ) using RPS is denoted as  $\hat{\mathbf{p}}_{RPSi}^{n+1}$  ( $\hat{\mathbf{p}}_{RPSj}^{n+1}$ ), the cooperative relative position of agent  $i$  based on vision data and RPS information from agent  $j$  is denoted as  $\tilde{\mathbf{p}}_{RPSi}^{n+1}$ , and the relative position for agent  $i$  using DRPS is denoted as  $\hat{\mathbf{p}}_{DRPSi}^{n+1}$ .

The local relative positioning (RPS) of each agent starts with the collection of a total of  $\mathbf{X}^n$  frequency sweeps (for a set of frequency bands  $M$ ), and for each frequency band the mean  $\psi_m^n$  is computed as:

$$\psi_m^n = \frac{1}{N_s} \sum_{n=1}^N \mathbf{X}_m^n \quad \forall m \in M, \tag{4}$$

where  $N_s = 1, \dots, N_F$ , and  $N_F$  denotes the total number of frequency sweeps conducted. Subsequently,  $\psi_m^n$  is used in conjunction with the path-loss, multilateration, LSQ, and discrete EKF (with sampling time  $T_s$ ) models and techniques as presented in [24] and summarized in Section 4, to extract the relative coordinates and obtain  $\hat{\mathbf{p}}$ .

To compute each agent’s relative position the state dynamics must be modeled, using a measurement and a motion model, with state vector  $\mathbf{p}^n = [p_R(1) \ p_R(2)]^T$  defined as the planar agent position. Thus, the posterior location esti-

mate using the agent’s dynamic model is given by:

$$\hat{\mathbf{p}}^{n+1} = \hat{\mathbf{p}}^n + T_s \begin{bmatrix} \cos \varphi^n & 0 \\ 0 & \sin \varphi^n \end{bmatrix} \left( \begin{bmatrix} u_x^n \\ u_y^n \end{bmatrix} + \mathbf{w}^n \right), \tag{5}$$

where  $\varphi^n$ ,  $u_x/u_y$ , and  $\mathbf{w}^n$  denote the agent’s heading angle, velocity, and process noise, respectively, with  $\mathbf{w}^n$  modeled by a normal distribution with a zero mean and covariance  $\mathbf{Q} = (0.1)\mathbf{I}_{2 \times 2}$ . Further, the measurement model is defined by:

$$\hat{\mathbf{d}}^{n+1} = \sqrt{(x_{land} - \hat{p}_R(1))^2 + (y_{land} - \hat{p}_R(2))^2} + v^n, \tag{6}$$

where the landmarks (i.e.,  $x_{land}$ ,  $y_{land}$ ) are obtained via RPS and  $v^n$  represents the zero mean noise measurement with constant covariance  $\mathbf{R} = (0.01)\mathbf{I}_{2 \times 2}$ .

For the calculation of  $\hat{\mathbf{p}}^{n+1} = f(\hat{\mathbf{p}}^n, \mathbf{u}^n)$  (i.e., the position estimate for time-step  $n + 1$ ), the motion model is used with:

$$\mathbf{F} = \frac{\partial f}{\partial \hat{\mathbf{p}}^{n+1}} |_{\hat{\mathbf{p}}^n, \mathbf{u}^n}, \tag{7}$$

as well as the measurement model  $\hat{\mathbf{d}}^{n+1} = h(\hat{\mathbf{p}}^n)$  with:

$$\mathbf{H} = \frac{\partial h}{\partial \hat{\mathbf{p}}^{n+1}} |_{\hat{\mathbf{p}}^n}. \tag{8}$$

Thus, the covariance for the system is given by:

$$\hat{\mathbf{P}}^{n+1} = \mathbf{F}\hat{\mathbf{P}}^n\mathbf{F}^T + \mathbf{Q}. \tag{9}$$

In summary, during the EKF prediction step,  $\varphi^n$  and  $u_x/u_y$ , measurements are used as input to the motion model that generates the agent’s state at time-step  $n$ . Consequently, the measurement model is used to compute the range between the different route points.

Afterwards, at the correction step the relative trajectory is generated, using the optical flow relative range measurements  $\mathbf{d}_{of}^{n+1}$ . Then, employing the Kalman gain  $\mathbf{K}$ , calculated as  $\mathbf{K} = \hat{\mathbf{P}}^{n+1}\mathbf{H}^T(\mathbf{H}\hat{\mathbf{P}}^{n+1}\mathbf{H}^T + \mathbf{R})^{-1}$ , the relative coordinates and the error covariance at time step  $n + 1$  can be computed as:

$$\hat{\mathbf{p}}^{n+1} = \hat{\mathbf{p}}^n + \mathbf{K}(\mathbf{d}_{of}^{n+1} - h(\mathbf{p}^n)), \tag{10}$$

$$\hat{\mathbf{P}}^{n+1} = (\mathbf{I} - \mathbf{K}\mathbf{H})\hat{\mathbf{P}}^n. \tag{11}$$

In an attempt to achieve online relative positioning, as discussed in Section 4.1.1, a frequency selection technique is utilized to compute the useful frequency bands set  $\mathbf{A}$ , and, as a consequence, the positions  $\hat{\mathbf{p}}$  are re-computed in an online fashion [36].

The update phase can occur when the sensors of agent  $i$  fail and the RPS-computed coordinates cannot meet the *mean range threshold requirement*,  $\bar{\mathbf{d}}$ , pre-set at the beginning

of the multi-agent operation, leading to the initiation of the distributed relative positioning methodology, so as to achieve a robust and precise relative positioning. In essence, as the drone moves it continuously obtains range measurements; if these measurements diverge (i.e., they are greater than the mean range measurement  $\bar{\mathbf{d}}$ ) this is an indication that a sensor malfunction probably occurred, thus initiating the distributed multi-agent localization procedure.

The first time the mean range requirement is not satisfied, the two autonomous agents exchange information regarding their position estimates in order to update them. In this case, agent  $i$  obtains a cooperative relative position estimation using vision data to compute the distance to (target) agent  $j$  in its vicinity, with respect to relative frame  $\mathcal{F}_{ij}$ , and RPS information from agent  $j$ :

$$\tilde{\mathbf{p}}_{RPSi}^{n+1} = \hat{\mathbf{p}}_{RPSj}^{n+1} - \mathbf{d}_c \quad \forall j \in J. \tag{12}$$

This measurement is utilized to update the relative position estimate of agent  $i$  in the distributed system and the covariance of this estimate is given as:

$$\tilde{\mathbf{F}} = \begin{bmatrix} \mathbf{F}_{ii} & 0 \\ 0 & \mathbf{F}_{jj} \end{bmatrix} \quad \forall j \in J, \tag{13}$$

$$\tilde{\mathbf{P}} = \begin{bmatrix} \hat{\mathbf{P}}_{ii} & \hat{\mathbf{P}}_{ij} \\ \hat{\mathbf{P}}_{ji} & \hat{\mathbf{P}}_{jj} \end{bmatrix} \quad \forall j \in J, \tag{14}$$

where,

$$\tilde{\mathbf{P}}_{ii}^n = \mathbf{F}_{ii} \hat{\mathbf{P}}_{ii} \mathbf{F}_{ii} + \mathbf{Q}_i, \tag{15}$$

$$\tilde{\mathbf{P}}_{ij}^n = \hat{\mathbf{P}}_{ii}^n \mathbf{S}_{ii}^{-1} \hat{\mathbf{P}}_{jj}^n + \mathbf{Q}_i \quad \forall j \in J, \tag{16}$$

with,

$$\mathbf{S}_{ii} = \mathbf{H} \hat{\mathbf{P}}^{n+1} \mathbf{H}^T + \mathbf{R}. \tag{17}$$

Also, the Kalman gain equation changes as:

$$\tilde{\mathbf{K}}_{ij} = \hat{\mathbf{P}}_{ij}^n \mathbf{H}_{ij}^T (\mathbf{H}_{ij} \hat{\mathbf{P}}_{ij}^n \mathbf{H}_{ij}^T + \mathbf{R}_i)^{-1} \quad \forall j \in J, \tag{18}$$

where,

$$\tilde{\mathbf{H}} = \begin{bmatrix} \mathbf{H}_{ii} & \mathbf{H}_{ij} \\ \mathbf{H}_{ji} & \mathbf{H}_{jj} \end{bmatrix} \quad \forall j \in J, \tag{19}$$

with matrices  $\mathbf{H}_{ii}$  and  $\mathbf{H}_{jj}$  computed in the self-localization scheme and  $\mathbf{H}_{ij}$  or  $\mathbf{H}_{ji}$  derived using the following equation:

$$\tilde{\mathbf{d}}_{DRPS}^{n+1} = \sqrt{(\tilde{p}_{RPSi}(1) - \tilde{p}_{RPSj}(1))^2 + (\tilde{p}_{RPSi}(2) - \tilde{p}_{RPSj}(2))^2 + v_i^n} \quad \forall j \in J. \tag{20}$$

For example,  $\mathbf{H}_{ij}$  can be obtained using  $\tilde{\mathbf{d}}_{DRPS}^{n+1} = h(\tilde{\mathbf{p}}_{RPS}^n)$  with:

$$\mathbf{H}_{ij} = \frac{\partial h}{\partial \tilde{\mathbf{p}}_{RPS}^{n+1}} \Big|_{\tilde{\mathbf{p}}_{RPS}^n} \quad \forall j \in J. \tag{21}$$

The final distributed relative position for agent  $i$  using DRPS is calculated as follows:

$$\tilde{\mathbf{p}}_{DRPSi}^{n+1} = \tilde{\mathbf{p}}_{RPSi}^n + \mathbf{K}_{ij}(\bar{\mathbf{d}} - h(\tilde{\mathbf{p}}_{RPS}^n)) \quad \forall j \in J. \tag{22}$$

In brief, an approximate distributed agent location is estimated using the RPS module of each agent, as well as various sensor modalities, in conjunction with an FSA to speed up the process. The relative coordinates for the autonomous agent  $i$  are computed by employing the shared information from target agents  $j \in J$  that are subsequently fused to achieve the DRPS-based trajectory estimation. The overall system’s architecture block diagram is illustrated in Fig. 5.

---

**Algorithm 1** DRPS Algorithm

---

- Input:** Relative RSS set of data obtained at each point in the route ( $\mathbf{X}^n$ )
- 1: Scan the frequency spectrum at agent’s current position for each transmitter  $T_k, k \in \mathcal{K}$
  - 2: **procedure** RPS
  - 3: Analyze  $\mathbf{X}^n$  and extract distribution moments  $\psi_m^n$
  - 4:  $\psi_m^n$  is used to calculate the relative distances using the path-loss model
  - 5: Apply multilateration
  - 6: Perform LSQ
  - 7: Concurrently, video stream acquisition from downward-facing camera at agent’s current position
  - 8:  $\mathbf{x}_{pixel}, \mathbf{y}_{pixel}$  computation
  - 9: GSD utilized for meters-to-pixel conversion
  - 10: Calc. avg. Euclidean distance  $\mathbf{d}_{of}$  over consecutive frames.
  - 11: Estimation of relative position  $\hat{\mathbf{p}}^n$  using EKF and best approximated solution,  $\mathbf{p}^*$ .
  - 12: When  $\bar{\mathbf{d}}$  requirement not met, information exchange starts
  - 13: **end procedure**
  - 14: **procedure** DISTRIBUTED RELATIVE POSITIONING
  - 15: The relative position estimate  $\tilde{\mathbf{p}}_{RPSi}^{n+1}$  is computed using the detection and tracking methodology Eq. 12
  - 16: Detection and tracking of the target agent(s)
  - 17: Calculation of depth distance and focal length
  - 18: Computation of horizontal distance
  - 19: Derivation of average of distances (for depth/horizontal, respectively) since the last RPS measurement
  - 20: Compute distance between agent  $i$  and all agents  $j \in J$  ( $\tilde{\mathbf{d}}_{DRPS}^{n+1}$ ) Eq. 20
  - 21: Use distributed EKF methodology to compute  $\tilde{\mathbf{p}}_{DRPSi}^{n+1}$  Eq. 22
  - 22: **end procedure**
  - 23: **Output:** DRPS relative trajectory
-

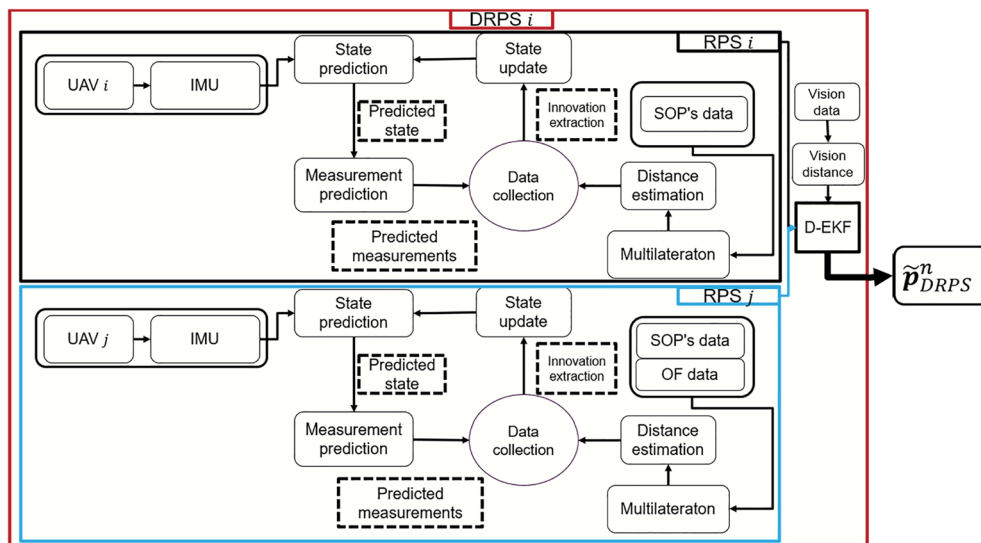


Fig. 5 DRPS architecture

## 7 Performance Evaluation

### 7.1 Hardware and Software Set-up

A 4G dongle is applied on each UAV agent of the system to allow the transmission and reception of both data and commands, while an SDR (the HackRF One, with specifications as detailed in <https://greatscottgadgets.com/hackrf/one/>) is used to scan the frequency spectrum and dynamically (online) receive the SOPs data. Note that the HackRF One is chosen for the implementation, as it has low cost, it requires a Linux operating system (Ubuntu in this implementation), and is programmable (utilizing a graphical block diagram interface, i.e., GNU Radio Companion or Python i.e., HackRF sweep) [56]. The proposed communication architecture, as

depicted in Fig. 6, is based on a virtual private network (VPN) server, enabling bidirectional communication between UAV agents via a client-to-client protocol. In this work, OpenVPN is employed due to its compatibility with the embedded Linux operating system. Figure 7 depicts the proposed system's current hardware/software implementation. In terms of hardware (Fig. 7 (top)), the NVIDIA Jetson Nano Developer Kit is employed as the processing unit onboard the agent that runs all algorithms and processes the collected data online.

Concerning the software implementation (Fig. 7 (bottom)), the Robot Operating System (ROS) [57] is used as middleware to enable interaction. Further, the ROS framework is utilized for the exchange of data between the agents, and the communication module runs on a fixed frequency to ensure online response onboard the agent.

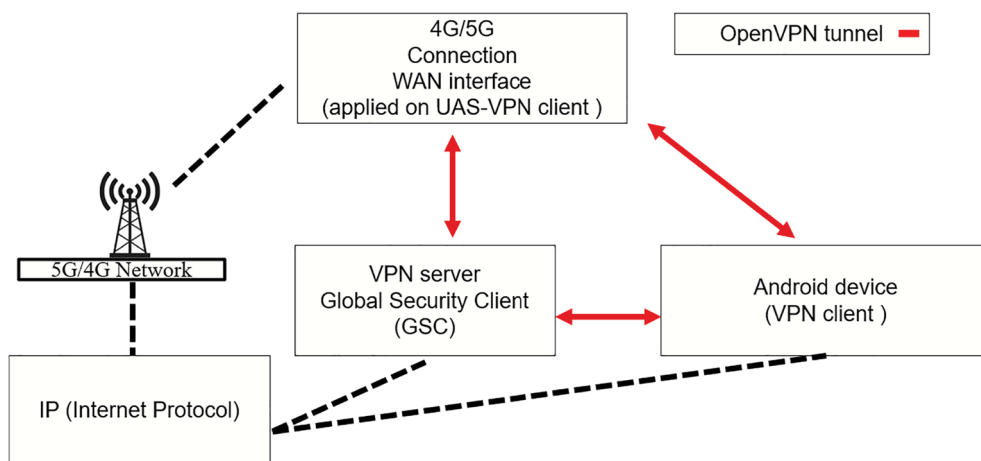


Fig. 6 Communication architecture

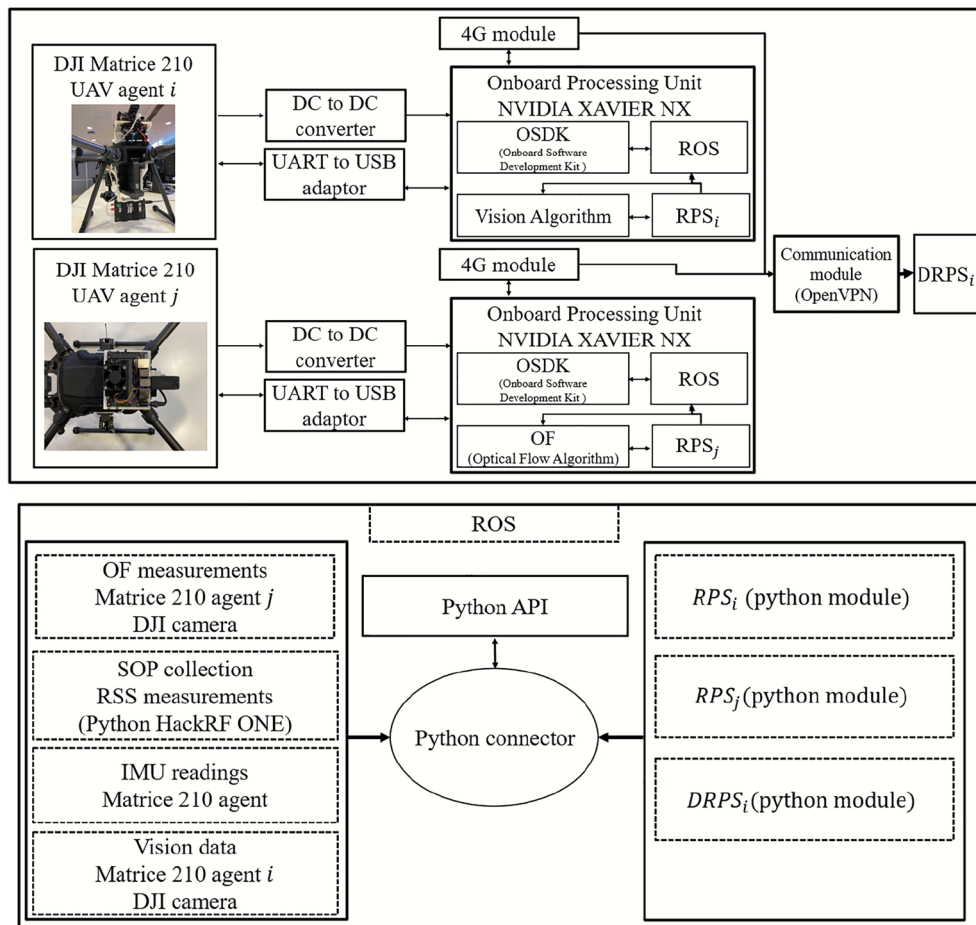


Fig. 7 (Top) Hardware implementation of the system; (Bottom) Software implementation of the system

Also, the performance of the communication framework is investigated (with additional outdoor experiments conducted). Figure 8 exhibits that the communication of the proposed multi-agent system can be continuously maintained online even at an altitude of 500 m and Euclidean distance from the remote controller of 2 km.

### 7.2 DRPS Experimentation

This section presents the DRPS experimental results by comparing the relative measurements for the agents employed, for each trajectory waypoint, with the ground truth (i.e., measurements acquired via GPS+IMU). In these experiments,

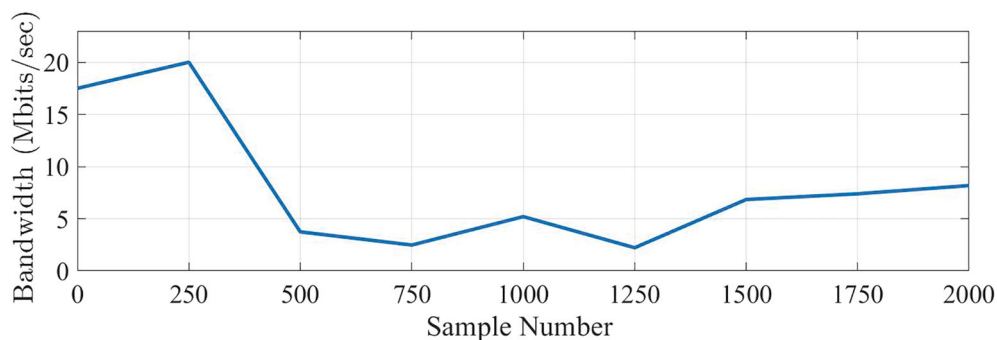


Fig. 8 DRPS bandwidth in a real-outdoor environment

the number of SOP transmitters utilized is  $|T_k| = 13$ , the value of the path loss exponent is  $n_{PL} = 2.8$ , and the frequency range is 0–3500 MHz, based on the analysis carried out in [24], which showed that for this frequency range, the system is able to converge to the relative coordinates over a short time period.

It should be noted that the outdoor experiments are conducted employing a limited number of autonomous UAV agents in the prototype implementation, due to the lack of additional SDR equipment and UAVs at our laboratory. Nevertheless, it is extremely important to implement the proposed system even for a small number of agents in both hardware and software, rather than performing only simulations as many of the approaches currently described in the literature, in order to demonstrate its feasibility with real-world experiments. Further, the outdoor experiments took place in an area that introduced challenges to commercial GNSS receivers, leading to GNSS positioning performance degradation due to the limited satellite visibility, multipath effect, interference, and other undesired obstacle obstructions (non-line-of-sight signals) [58, 59]. Thus, to counter these issues, the proposed multi-agent system is utilized, which demonstrates reliable and robust location estimation.

First, a performance analysis concerning the detection and tracking modules is presented, with Fig. 9 demonstrating that the DRPS agents are able to detect-and-track a drone up to a Euclidean distance of 93 m. In addition, it is demonstrated

that the vision+OF data can provide a 94% drone detection rate (contrary to the vision-only approach that demonstrated a 70% detection rate).

Specifically, a neural network is trained, with performance metrics related to training, validation, and testing as depicted in Fig. 10. The neural network is then employed to detect a rogue drone in images in conjunction with the computation and projection of the visual target's position relative change in a 2D space (based on an observer).

Further, the relative paths computed for different UAV agents using various positioning techniques for a specific path comprised of three straight lines are presented in Fig. 11. For this path, Table 1 tabulates the real and relative trajectories obtained online when using the RPS and DRPS techniques. These results demonstrate that the RPS technique encounters sensor shortfalls in the outdoor experiments, which leads to a decreased relative positioning performance when compared to DRPS. As shown, the DRPS technique that uses SOPs, in conjunction with IMU, optical flow, and vision data, can estimate the agent's route in a reliable and accurate manner, generating a relative trajectory with distances that are analogous to the ground truth (i.e., the GPS+IMU trajectory). Thus, by employing a distributed localization technique, robust online localization in GNSS-challenged areas can be obtained.

Specifically, 70 outdoor experiments have been conducted in order to compute the detector performance, as well as the distributed relative localization performance. It must be

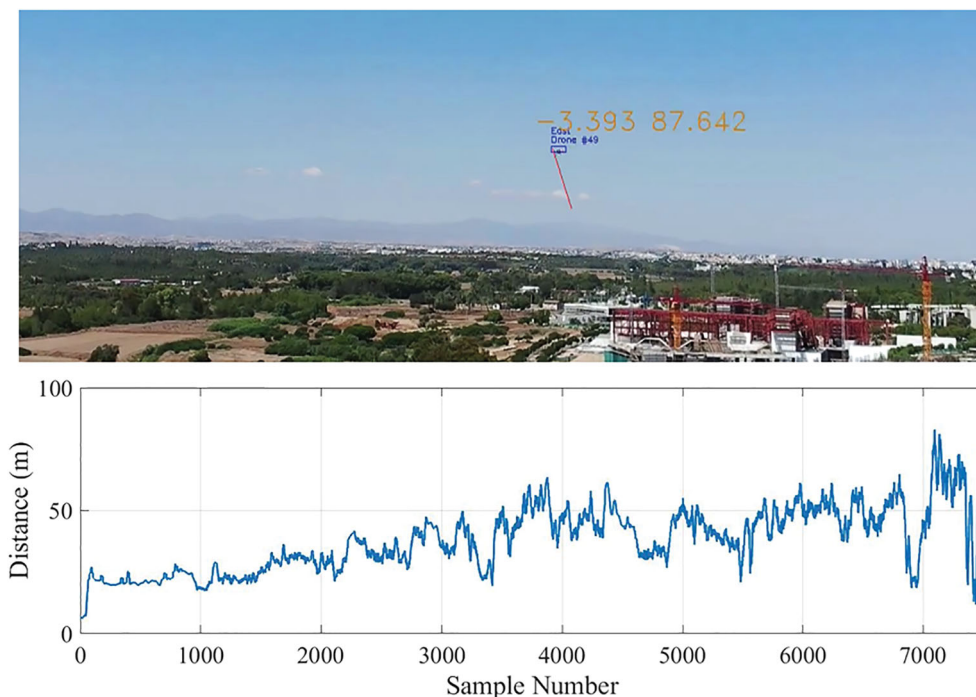


**Fig. 9** Tracking performance over distance (in meters)



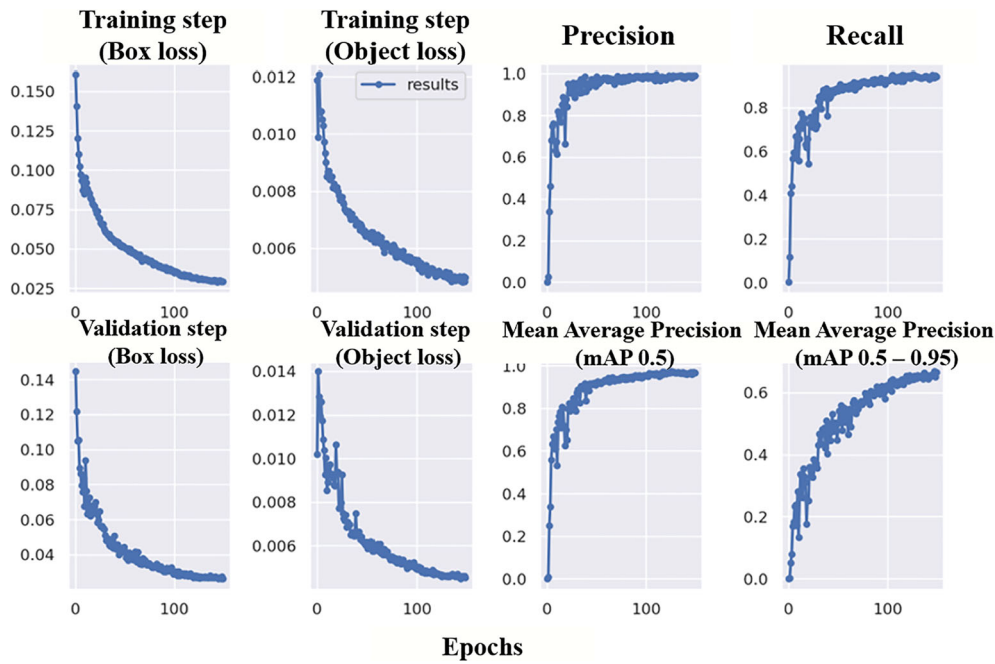


Fig. 10 Detector performance metrics

noted that Fig. 11 presents the relative trajectories computed using the RPS and DRPS in comparison to the GPS+IMU (GT). The letter tags in Fig. 11 denote the trajectory segments that are also tabulated in Table 1, illustrating the relative localization performance of RPS and DRPS compared to the GT value (GPS+IMU) by calculating the Euclidean distance between points A-D (with the formula deployed for the difference computation on Table 1 given by:  $(GT \text{ value} - \text{estimated value})100/ GT \text{ value}$ ). Further, as shown in Table 1, for RPS the error accumulates as the UAV moves from one trajectory point to another; on the contrary, for DRPS the accumulation error is reduced due to the sensor data fusion of multiple agents (vision, optical flow, SOP, and IMU data from multiple agents are employed to achieve improved relative localization performance).

Apart from the relative trajectories associated with each agent, the route variations between real and relative trajectories obtained by the RPS and DRPS techniques, are shown in Fig. 12. The increase in accuracy and reliability of DRPS compared to RPS is evident in Fig. 12(a), as the minimum

square error (MSE) of DRPS is lower compared to RPS. Clearly, for the relative positioning of agent  $i$ , when there are insufficient sample data, or the sensor information deteriorates, distributed positioning is a necessity, as the utilization of the RPS data from agents  $j \in J$  in its vicinity can compensate for the lack of self-localization information. This is also demonstrated in Fig. 12(b), that utilizes a cumulative distribution function (CDF) plot to show that the localization error (Euclidean distance) of DRPS is 75% of the time less than 6 m as compared to GPS+IMU. On the contrary, the RPS error reaches a value greater than 10 m.

Even though EKF is defined as a powerful state estimator, the noise covariances need to be computed based on the sensor outputs [60]. However, process and measurement noise covariances may not be accurately computed due to partially known parameters (such as the environmental conditions), thus affecting the system’s performance in practical scenarios [61]. In this work, the process and measurement noise covariances are determined/tuned based on the sensor outputs and by computing the mean deviation between

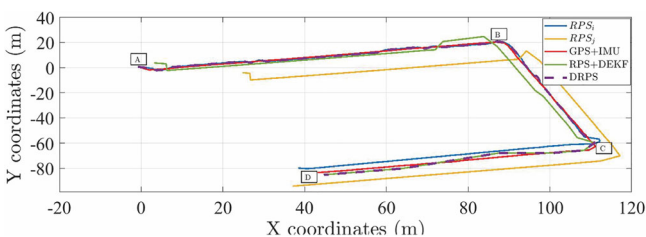
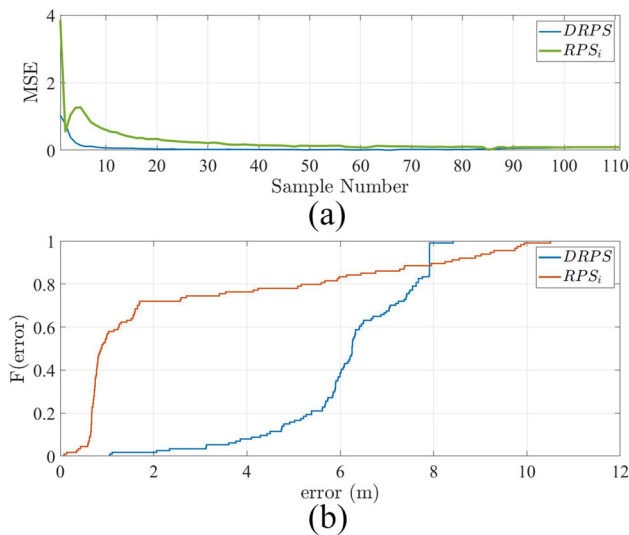


Fig. 11 DRPS and RPS relative trajectories compared to GPS+IMU

Table 1 Online Experiment - Trajectory Distances

Trajectory Segments	A-B(m)/ Dif.(%)	B-C(m)/ Dif.(%)	C-D(m)/ Dif.(%)
GPS+IMU	107/0	110/0	83/0
GNSS distance	105/1.87	107.5/2.27	81/2.4
Relative distance (RPS)	105/1.87	104/5.45	75/9.6
Relative distance (DRPS)	106/1	107/2.72	81.5/1.8



**Fig. 12** (a) MSE (in meters) of RPS and DRPS vs. GPS+IMU (b) Position estimation error CDF for RPS and DRPS

the motion and measurement models from the ground truth (in real outdoor experiments). Specifically, for the proposed system, the process and measurement covariance matrices are set as  $\mathbf{Q} = (0.1)\mathbf{I}_{2 \times 2}$  and  $\mathbf{R} = (0.01)\mathbf{I}_{2 \times 2}$  (with process noise  $\mathbf{w} = 0.316$  and measurement noise  $\nu = 0.1$ ), respectively. Figure 13 depicts the performance of DRPS with the use of different covariance matrices, illustrating that those parameters can impact the system’s localization performance (2-norm error). Further, it validates the choice of parameters utilized in this work.

Additionally, a statistical analysis is also carried out to further examine the DRPS performance in comparison to both the RPS approach [24] and the ground truth (fused GPS+IMU). Figure 14 illustrates the 2-norm (m) deviation from the GPS+IMU dataset of the relative trajectories derived by implementing DRPS and RPS. As demonstrated, DRPS delivers reliable and higher accuracy localization compared to RPS, as the Euclidean error (2-norm) of the relative path computed is significantly smaller (i.e., the maximum error for DRPS is up to 8 m, compared to RPS with a maximum error reaching 11 m).

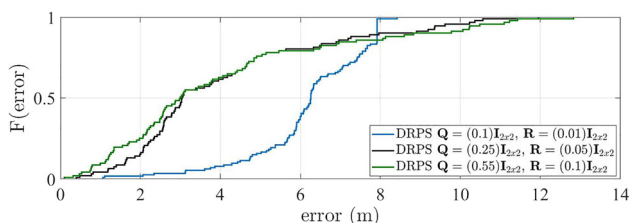


**Fig. 13** Position estimation error CDF, using different process and measurement noise covariance parameters

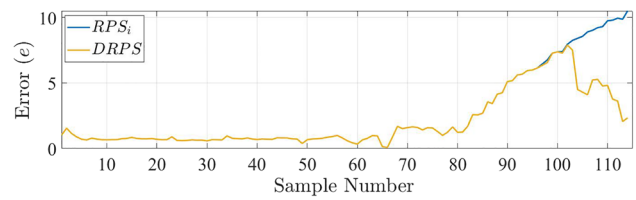


**Fig. 14** Euclidean distance comparison of DRPS, and RPS using GPS+IMU as the ground truth

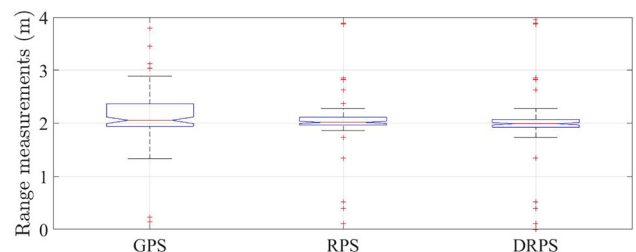
Moreover, Fig. 15 illustrates the boxplots of the various positioning systems (i.e., the median, maximum, and minimum values), demonstrating that the DRPS median is close to the ground-truth (GPS+IMU dataset).

Figure 16 presents the average covariance and mean statistics of the localization states, again demonstrating the enhanced performance of DRPS compared to RPS.

Furthermore, to evaluate the performance of DRPS when SOP disturbances and IMU drift are present, outdoor experiments (in a deep urban area) with the same configuration parameters are conducted. Figure 17 illustrates that without the use of the proposed DRPS framework, agent  $i$  is not able to counteract the IMU data drift caused by the presence of SOP disturbances and the prolonged period of location estimation. The SOPs’ erroneous information leads to significant deviation from the GT (GPS+IMU).

To present the difference in terms of localization when different methodologies (odometry and visual odometry (INS, INS+OF techniques)) are in use, the mean absolute error (MAE) for 70 outdoor experiments within the same environment is tabulated in Table 2, again showing that the DRPS-based relative positioning and navigation are more accurate. Also, the DRPS produced more accurate results compared to SLAM-based techniques, where the localization error after 30 seconds of GPS unavailability led to an error up to 50 m, due to INS drift during prolonged periods [23, 62].

In addition to the tabulated positioning techniques, the DRPS can be compared with anchor-based localization techniques. As described in Section 2, UWB tags can be used as anchors whose positions are already known in advance



**Fig. 15** Statistical comparison of GPS, DRPS, and RPS. Range measurements are defined as the UAV distances covered from one waypoint to another

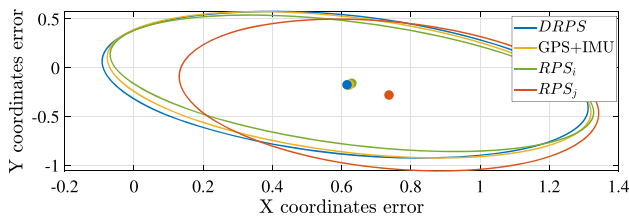


**Fig. 16** Banana-shaped covariance ellipsoids showing the final pose and uncertainty related to RPS, DRPS, and GPS+IMU

to achieve accurate positioning [63]. However, the UWB anchors in outdoor environments are not easily employed, as the distance between Tx and Rx is up to 50 m and very large errors are unavoidable in non-line-of-sight conditions [64–66]. Further, as shown in [67], for the TDOA method, a technique that requires the locations of anchor points, the time that the signals are received and the traveling speed of those signals can be employed for accurate location estimation. However, even though the TDOA method can achieve high accuracy levels in terms of root mean square error (RMSE), employing various scenarios (Monte-Carlo simulations) using multiple drones, the results for this technique presented cases where the error exceeded 50 m (contrary to DRPS where the error does not exceed 8 m). In [3], to investigate collaborative localization when event-based communication and SOPs are in use, two UAVs were deployed in outdoor experiments along with pseudorange methodology to obtain a root mean square error (RMSE) of 11 m, while DRPS performance analysis shows a RMSE in the range of 5 m (for 70 outdoor experiments). Also, the DRPS produces more accurate results when compared to an SOP-based positioning method, as described in [2], that employed asynchronous radio transmissions from fixed stations and mobile GPS-equipped nodes to cooperatively localize a blind node, with the DRPS achieving localization performance with 2-

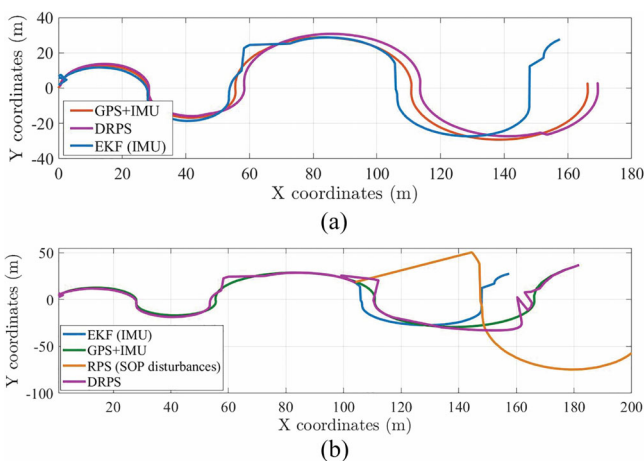


**Fig. 17** Relative localization performance evaluation with the presence of (a) IMU drift and (b) SOP disturbances compared with DRPS

**Table 2** Mean absolute error of GNSS, INS, OF, RPS, and DRPS techniques

#	GNSS	INS	OF	RPS	DRPS	MAE (meters)
1	x					4.5
2		x				21
3		x	x			16
4				x		9.7
5					x	5.5

norm error lower than 8 m, as compared to [2] where the 2-norm position error was in the range of 30 m. In addition, the DRPS is compared with cooperative tracking by multi-agent systems using SOPs. Specifically, the authors in [68], proposed a cooperative framework that investigated the performance bounds of cooperative tracking using SOPs by multiple asynchronous agents equipped with antenna arrays and it is demonstrated that DRPS outperforms the proposed system with RMSE in the range of 5 m compared to a RMSE of 10 m for the system in [68]. Further, the work in [69] demonstrated a 2-norm error in the range of 10 m using collaborative bathymetry-based localization, while DRPS illustrates lower 2-norm error (in the range of 8 m).

It should be noted that the outdoor experiments are conducted employing two autonomous UAV agents in the prototype implementation, due to the limited number of available SDR equipment and UAV agents. However, as it is important to validate the scalability of the proposed system, additional UAV agents are simulated employing the DJI drone simulator (due to computing hardware requirements, two, four, and six agents are simulated; however, this scheme can potentially scale to much larger swarms, with the only limitation being the utilization of appropriate hardware/software on each agent to support the multi-agent system). Performance results obtained demonstrate that the proposed system’s relative localization performance improves as the number of agents increases (Fig. 18).

To further evaluate the performance of DRPS, more flight routes are also considered, and it is demonstrated that the proposed system is still able to estimate the UAV agent’s position under erroneous sensor measurement cases, in non-complex as well as more complex routes (see Fig. 19).

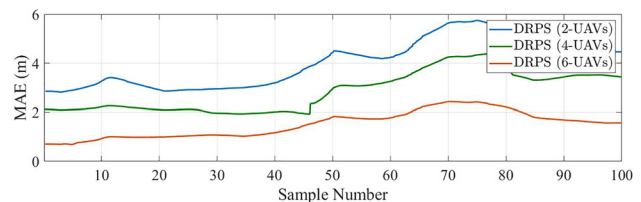


**Fig. 18** MAE of DRPS vs. GPS+IMU using different number of agents

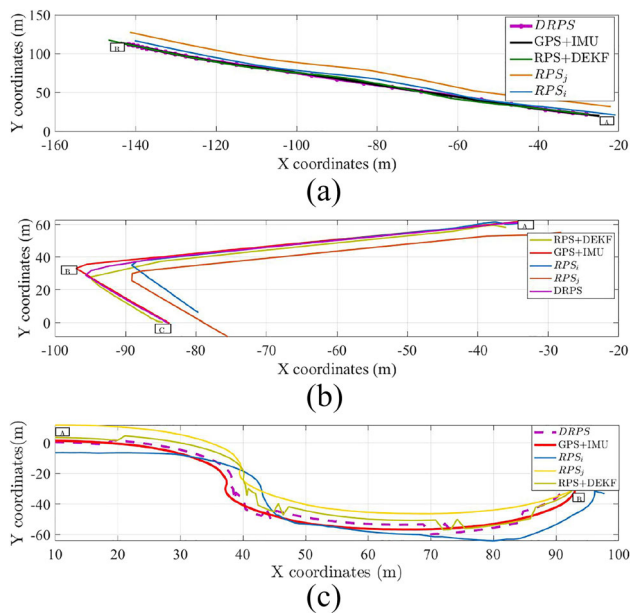


**Fig. 19** UAV agent's position under erroneous sensor measurement cases for various flight routes

Finally, the RPS and DRPS techniques are compared in terms of reliability over numerous outdoor experiments. The proposed system reproduces distributed relative positioning under specifically defined conditions in 70 outdoor experiments, indicating a 95% accurate location fix (as compared to 70% for RPS). In this work, an accurate location fix is defined as the ability to accurately estimate the UAV agent's position (i.e., having a localization error of less than 10 m and a complete UAV waypoint path).

## 8 Conclusions

This work proposes a novel online distributed navigation system (DRPS). The UAV agents are able to exploit the SOPs (without the need for the transmitter locations), along with information from various other sensor modalities (i.e., visual, optical flow, and IMU), independently for self-localization. Further, when GNSS signals are not available or in case of sensor faults, each agent in the system employs the knowledge from other agents in its vicinity in order to achieve robust relative positioning. Such a system, that entails communicating and fusing information exchanged between multiple agents can be adopted in case of jamming or spoofing attacks, in order to achieve efficient and reliable navigation incorporating a relative trajectory. An extensive assessment of the system in real outdoor scenarios showcased its ability to cope with GNSS signal shortfalls, demonstrating that the DRPS technique can obtain robust online relative localization and can be used as a positioning alternative, with

results comparable to the state-of-the-art fused GPS+IMU performance.

Future work will address the issues of localization precision with the fusion of 5G information (with various methods such as ToA and AoA). Further, ongoing research includes deep learning and TDOA information fusion techniques to mitigate the accumulated error from the various sensors in long-term operations, achieving more precise navigation.

**Acknowledgements** This work has been supported by the European Union's Horizon 2020 research grant agreement 739551 (KIOS CoE - TEAMING) and from the Republic of Cyprus through the Deputy Ministry of Research, Innovation and Digital Policy

**Author Contributions** All authors contributed to the study's conception and design in an equal manner. Material preparation, analysis, and implementation were performed by Nicolas Souli.

**Funding** Open access funding provided by the Cyprus Libraries Consortium (CLC). This work was supported by the European Union's Horizon 2020 research and innovation program under grant agreements No 101017258 (SESAME) and No 739551 (KIOS CoE - TEAMING) and from the Republic of Cyprus through the Deputy Ministry of Research, Innovation and Digital Policy.

**Availability of data and material** Not applicable

**Code Availability** Not applicable

## Declarations

**Conflicts of interest/Competing interests** No Conflicts of interest

**Ethics approval** Not applicable

**Consent to participate** Not applicable

**Consent for publication** Not applicable

**Open Access** This article is licensed under a Creative Commons Attribution 4.0 International License, which permits use, sharing, adaptation, distribution and reproduction in any medium or format, as long as you give appropriate credit to the original author(s) and the source, provide a link to the Creative Commons licence, and indicate if changes were made. The images or other third party material in this article are included in the article's Creative Commons licence, unless indicated otherwise in a credit line to the material. If material is not included in the article's Creative Commons licence and your intended use is not permitted by statutory regulation or exceeds the permitted use, you will need to obtain permission directly from the copyright holder. To view a copy of this licence, visit <http://creativecommons.org/licenses/by/4.0/>.

## References

1. Maaref, M., Kassas, Z.M.: Ground vehicle navigation in GNSS-challenged environments using signals of opportunity and a closed-loop map-matching approach. *IEEE Trans. Intell. Transport. Syst.* **21**, 2723–2738 (2019)
2. Coluccia, A., Ricciato, F., Ricci, G.: Positioning based on signals of opportunity. *IEEE Commun. Lett.* **18**, 356–359 (2014)



3. Morales, J., Kassas, Z.M.: Event-based communication strategy for collaborative navigation with signals of opportunity. In: Proc. Asilomar Conf. on Signals, Systems, and Computers (2018)
4. Maaref, M., Khalife, J., Kassas, Z.M.: Lane-level localization and mapping in GNSS-challenged environments by fusing lidar data and cellular pseudorange. *IEEE Trans. Intell. Veh.* **4**, 73–89 (2018)
5. Angelino, C.V., Baraniello, V.R., Cicala, L.: UAV position and attitude estimation using IMU, GNSS and camera. In: Proc. Int. Conf. on Inf. Fusion (2012)
6. Simkovits, H., Weiss, A.J., Amar, A.: Navigation by inertial device and signals of opportunity. *Signal Process.* **131**, 280–287 (2017)
7. Shamaei, K., Khalife, J., Kassas, Z.M.: Exploiting LTE signals for navigation: Theory to implementation. *IEEE Trans. Wireless Commun.* **17**, 2173–2189 (2018)
8. Kassas, Z.Z.M., Khalife, J., Shamaei, K., Morales, J.: I hear therefore I know where I am: Compensating for GNSS limitations with cellular signals. *IEEE Signal Process. Mag.* **34**, 111–124 (2017)
9. Michel, A.H.: Counter-drone systems. Center for the Study of the Drone at Bard College. <https://dronecenter.bard.edu/files/2019/12/CSD-CUAS-2nd-Edition-Web.pdf> (2019). Accessed 15 January 2023
10. Bresson, G., Alsayed, Z., Yu, L., Glaser, S.: Simultaneous localization and mapping: A survey of current trends in autonomous driving. *IEEE Trans. Intell. Veh.* **2**, 194–220 (2017)
11. Kapoor, R., Ramasamy, S., Gardi, A., Sabatini, R.: UAV navigation using signals of opportunity in urban environments: A review. *Energy Procedia* **110**, 377–383 (2017)
12. Cooper, A.J., Redman, C.A., Stoneham, D.M., Gonzalez, L.F., Etse, V.K.: A dynamic navigation model for unmanned aircraft systems and an application to autonomous front-on environmental sensing and photography using low-cost sensor systems. *Sensors* **15**, 21537–21553 (2015)
13. Morales, J.J., Kassas, Z.M.: Distributed signals of opportunity aided inertial navigation with intermittent communication. In: Proc. Int. Techn. Mtg. Satellite Div. Inst. of Navigat. (2018)
14. Raquet, J.F., Miller, M.M.: Issues and approaches for navigation using signals of opportunity. In: Proc. National Technical Meeting of The Inst. of Navigat. (2007)
15. Raquet, J.F.: Navigation using pseudolites, beacons, and signals of opportunity. In: NATO STO Lecture Series SET-197, Navigat. Sensors and Syst. in GNSS Degraded and Denied Environm. (2013)
16. Zwirello, L., Li, X., Zwick, T., Ascher, C., Werling, S., Trommer, G.F.: Sensor data fusion in UWB-supported inertial navigation systems for indoor navigation. In: Proc. IEEE Int. Conf. Robot. Autom. (ICRA) (2013)
17. Zingg, S., Scaramuzza, D., Weiss, S., Siegwart, R.: MAV navigation through indoor corridors using optical flow. In: Proc. IEEE Int. Conf. Robot. Autom. (ICRA) (2010)
18. Shen, C., Bai, Z., Cao, H., Xu, K., Wang, C., Zhang, H., Wang, D., Tang, J., Liu, J.: Optical flow sensor/INS/magnetometer integrated navigation system for MAV in GPS-denied environment. *J. Sensors* **2016**, 1–11 (2016)
19. Schmuck P., Chli, M.: Multi-UAV collaborative monocular SLAM. In: Proc. IEEE Int. Conf. Robot. Autom. (ICRA) (2017)
20. Karrer, M., Agarwal, M., Kamel, M., Siegwart, R., Chli, M.: Collaborative 6DoF relative pose estimation for two UAVs with overlapping fields of view. In: Proc. IEEE Int. Conf. Robot. Autom. (ICRA) (2018)
21. Liu, R., Yuen, C., Do, T-N., Jiao, D., Liu, X., Tan, U-X.: Cooperative relative positioning of mobile users by fusing IMU inertial and UWB ranging information. In: Proc. IEEE Int. Conf. Robot. Autom. (ICRA) (2017)
22. Piasco, N., Marzat, J., Sanfourche, M.: Collaborative localization and formation flying using distributed stereo-vision. In: Proc. IEEE Int. Conf. Robot. Autom. (ICRA) (2016)
23. Karrer, M., Chli, M.: Towards globally consistent visual-inertial collaborative SLAM. In: Proc. IEEE Int. Conf. Robot. Autom. (ICRA) (2018)
24. Souli, N., Kolios, P., Ellinas, G.: Relative positioning of autonomous systems using signals of opportunity. In: Proc. IEEE Veh. Technol. Conf. (VTC2020-Spring) (2020)
25. Souli, N., Kolios, P., Ellinas, G.: Online relative positioning of autonomous vehicles using signals of opportunity. *IEEE Trans. Intell. Veh.* **7**, 873–885 (2022)
26. Xu, Y., Ou, Y., Xu, T.: SLAM of robot based on the fusion of vision and LIDAR. In: Proc. IEEE Int. Conf. on Cyborg and Bionic Systems (CBS) (2018)
27. Meronen, L., Wilkinson, W.J., Solin, A.: Movement tracking by optical flow assisted inertial navigation. In: Proc. IEEE Int. Conf. on Inf. Fusion (2020)
28. Song, Y., Guan, M., Tay, W.P., Law, C.L., Wen, C.: UWB/LiDAR fusion for cooperative range-only SLAM. In: Proc. IEEE Int. Conf. Robot. Autom. (ICRA) (2019)
29. Moon, S., Youn, W.: A novel movable UWB localization system using UAVs. *IEEE Access* **10**, 41303–41312 (2022)
30. Queralt, J.P., Martínez Almansa, C., Schiano, F., Floreano, D., Westerlund, T.: UWB-based system for UAV localization in GNSS-denied environments: Characterization and dataset. In: Proc. IEEE/RSJ Int. Conf. on Intelligent Robots and Systems (IROS) (2020)
31. Bailey, T., Bryson, M., Mu, H., Vial, J., McCalman, L., Durrant-Whyte, H.: Decentralised cooperative localisation for heterogeneous teams of mobile robots. In: Proc. IEEE Int. Conf. Robot. Autom. (ICRA) (2011)
32. Souli, N., Makrigiorgis, R., Kolios, P., Ellinas, G.: Cooperative relative positioning using signals of opportunity and inertial and visual modalities. In: Proc. IEEE Veh. Technol. Conf. (VTC2021-Spring) (2021)
33. Powell, W., Ryzhov, I.: *Optimal Learning*. Wiley, Hoboken, NJ (2012)
34. Frazier, P., Powell, W., Dayanik, S.: The knowledge-gradient policy for correlated normal beliefs. *INF. J. Comput.* **21**, 599–613 (2009)
35. Ryzhov, I., Powell, W.B., Frazier, P.I.: The knowledge gradient algorithm for a general class of online learning problems. *Oper. Res.* **60**, 180–195 (2012)
36. Souli, N., Kolios, P., Ellinas, G.: Adaptive frequency band selection for accurate and fast positioning utilizing SOPs. In: Proc. IEEE International Conference on Unmanned Aircraft System (ICUAS) (2022)
37. Li, G., Geng, E., Ye, Z., Xu, Y., Lin, J., Pang, Y.: Indoor positioning algorithm based on the improved RSSI distance model. *Sensors* **18**, 1–15 (2018)
38. Ge, B., Han, J., Zhao, B.: Improved RSSI positioning algorithm for coal mine underground locomotive. *J. Electr. Comp. Eng.* **2015**, 1–8 (2015)
39. Tomic, S., Beko, M., Dinis, R., Bernardo, L.: On target localization using combined RSS and AoA measurements. *Sensors* **18**, 1–25 (2018)
40. International Telecommunication Union: Technical and operating parameters and spectrum use for shortrange radio communication devices. ITU-R SM.2153-8. [https://www.itu.int/dms\\_pub/itu-r/opb/rep/R-REP-SM.2153-9-2022-PDF-E.pdf](https://www.itu.int/dms_pub/itu-r/opb/rep/R-REP-SM.2153-9-2022-PDF-E.pdf) (2021). Accessed 15 January 2023
41. Federal Communications Commission: Study of digital television field strength standards and testing procedures. Report To Congress, ET Docket No. 05-182. <https://transition.fcc.gov/oet/info/documents/reports/SHVERA/SHVERA-FCC-05-199.pdf> (2005). Accessed 15 January 2023
42. International Telecommunication Union: Impact of audio signal processing and compression techniques on terrestrial FM sound broadcasting emissions at VHF. ITU-R BS.2213-



4. [https://www.itu.int/dms\\_pub/itu-r/opb/rep/R-REP-BS.2213-4-2017-PDF-E.pdf](https://www.itu.int/dms_pub/itu-r/opb/rep/R-REP-BS.2213-4-2017-PDF-E.pdf) (2017). Accessed 15 January 2023
43. Abhayawardhana, V.S., Wassell, I.J., Crosby, D., Sellars, M.P., Brown, M.G.: Comparison of empirical propagation path loss models for fixed wireless access systems. In: Proc. IEEE Veh. Techn. Conf. (2005)
  44. Ismail, M.: An RSSI-based wireless sensor node localisation using trilateration and multilateration methods for outdoor environment. [arXiv:1912.07801](https://arxiv.org/abs/1912.07801) [eess.SP] (2019)
  45. Wang, Y., Yang, X., Zhao, Y., Liu, Y., Cuthbert, L.: Bluetooth positioning using RSSI and triangulation methods. In: Proc. IEEE Consumer Commun. Netw. Conf. (2013)
  46. Silva, H.: Experimental study on RSS based indoor positioning algorithms. In: Yang, G.C., Ao, S.I., Gelman, L. (eds.) Transactions on Engineering Technologies, pp. 451–466. Springer, Dordrecht (2015)
  47. Lee, H.: A novel procedure for assessing the accuracy of hyperbolic multilateration systems. *IEEE Trans. Aerosp. Electron. Syst.* **AES-11**, 2–15 (1975)
  48. Brown, R., Hwang, P.: Introduction to Random Signals and Applied Kalman Filtering with MatLab Exercises. Wiley, New York (2011)
  49. Sazdovski, V., Kolemishvska-Gugulovska, T., Stankovski, M.: Kalman filter implementation for unmanned aerial vehicles navigation. *IFAC Proc. Volumes* **38**, 12–17 (2005)
  50. Wickert, M., Siddappa, C.: Exploring the extended Kalman filter for GPS positioning using simulated user and satellite track data. In: Proc. Python in Science Conf. (2018)
  51. Maaloul, B., Taleb-Ahmed, A., Niar, S., Harb, N., Valderrama, C.: Adaptive video-based algorithm for accident detection on highways. In: Proc. IEEE Int. Symp. on Industrial Embedded Systems (2017)
  52. Sigut, J., Castro, M., Arnay, R., Sigut, M.: OpenCV basics: A mobile application to support the teaching of computer vision concepts. *IEEE Trans. Educ.* **63**, 328–335 (2020)
  53. Valenzuela, A.Q., Reyes, J.: Basic spatial resolution metrics for satellite imagers. *IEEE Sensors J.* **19**, 4914–4922 (2019)
  54. Bochkovskiy, A., Wang, C.-Y., Liao, H.-Y.M.: YOLOv4: Optimal speed and accuracy of object detection. [arXiv:2004.10934](https://arxiv.org/abs/2004.10934) [cs.CV] (2020)
  55. Makrigorgis, R., Kolios, P., Timotheou, S., Theocharides, T., Panayiotou, C.G.: Extracting the fundamental diagram from aerial footage. In: Proc. IEEE Veh. Technol. Conf. (VTC2020-Spring) (2020)
  56. Martoyo, I., Setiasabda, P., Kanalebe, H.Y., Uranus, H.P., Pardede, M.: Software defined radio for education: Spectrum analyzer, FM receiver/transmitter and GSM sniffer with HackRF One. In: Proc. Borneo Int. Conf. on Applied Math. and Eng. (2018)
  57. Quigley, M., Gerkey, B., Conley, K., Faust, J., Foote, T., Leibs, J., Berger, E., Wheeler, R., Ng, A.: ROS: An open-source robot operating system. In: Proc. ICRA Workshop on Open Source Software (2009)
  58. Zhu, N., Marais, J., Bétaille, D., Berbineau, M.: GNSS position integrity in urban environments: A review of literature. *IEEE Trans. Intell. Transp. Syst.* **19**, 2762–2778 (2018)
  59. Zidan, J., Adegoke, E.I., Kampert, E., Birrell, S.A., Ford, C.R., Higgins, M.D.: GNSS vulnerabilities and existing solutions: A review of the literature. *IEEE Access* **9**, 153960–153976 (2021)
  60. Ge, Q., Shao, T., Duan, Z., Wen, C.: Performance analysis of the Kalman filter with mismatched noise covariances. *IEEE Trans. Autom. Contr.* **61**, 4014–4019 (2016)
  61. Saito, A., Kizawa, S., Kobayashi, Y., Miyawaki, K.: Pose estimation by extended Kalman filter using noise covariance matrices based on sensor output. *ROBOMECH J.* **7**, 1–11 (2020)
  62. Morales, J., Kassas, Z.M.: Information fusion strategies for collaborative radio SLAM. In: Proc. IEEE/ION Position, Location and Navigation Symposium (PLANS) (2018)
  63. Ferrigno, L., Miele, G., Milano, F., Pingerna, V., Cerro, G., Laracca, M.: A UWB-based localization system: analysis of the effect of anchor positions and robustness enhancement in indoor environments. In: Proc. IEEE Int. Instrumentation and Measurement Technology Conf. (I2MTC) (2021)
  64. Shi, Q., Zhao, S., Cui, X., Lu, M., Jia, M.: Anchor self-localization algorithm based on UWB ranging and inertial measurements. *Tsinghua Sci. Technol.* **24**, 728–737 (2019)
  65. Kolakowski, J., Consoli, A., Djaja-Josko, V., Ayadi, J., Moriggia, L., Piazza, F., UWB localization in EIGER indoor/outdoor positioning system. In: Proc. IEEE Int. Conf. on Intelligent Data Acquisition and Advanced Computing Systems: Technology and Applications (IDAACS) (2015)
  66. Li, Y., Maorong, J., Qiang, L., Guili, Y., Kai, D.: Research on the IR-UWB ranging algorithm in outdoor near-ground environment. In: Proc. Int. Conf. on Sensor Networks and Signal Processing (SNSP) (2018)
  67. Wang, W., Bai, P., Liang, X., Zhang, J., He, L.: Performance analysis for TDOA localization using UAVs with flight disturbances. In: Proc. Int. Conf. on Inf. Fusion (2017)
  68. Wang, Y., Wu, Y., Shen, Y.: Cooperative tracking by multi-agent systems using signals of opportunity. *IEEE Trans. Coms.* **68**, 93–105 (2020)
  69. Teck, T. Y., Chitre, M., Hover, F. S.: Collaborative bathymetry-based localization of a team of autonomous underwater vehicles. In: Proc. IEEE International Conference on Robotics and Automation (ICRA) (2014)

**Publisher's Note** Springer Nature remains neutral with regard to jurisdictional claims in published maps and institutional affiliations.

**Nicolas Souli** received his B.Sc. degree in Electrical Engineering from the Cyprus University of Technology (2016) and his M.Sc. degree in Biomedical Engineering from Imperial College London (2017). He received his Ph.D. degree in Electrical and Computer Engineering from University of Cyprus (2023). His research focus is on the operation of autonomous agents, signal processing and telecommunication networks.

**Panayiotis Kolios** received the B.Eng. (2008) and Ph.D. (2011) degrees in Telecommunications Engineering from King's College London. He is a Research Assistant Professor with the KIOS Research and Innovation Center of Excellence, University of Cyprus. His interests focus on both basic and applied research on networked intelligent systems. Examples of such systems include intelligent transportation systems, autonomous unmanned aerial systems, and the plethora of cyber-physical systems that arise within IoT.

**Georgios Ellinas** holds a B.S., M.Sc., M.Phil., and a Ph.D. in Electrical Engineering from Columbia University. He is a Professor at the ECE Department and a founding member of the KIOS Research and Innovation Center of Excellence at the University of Cyprus. Prior to joining the University of Cyprus Dr. Ellinas also served as an Associate Professor of Electrical Engineering at City College of the City University of New York, as a Senior Network Architect at Tellium Inc., and as a Research Scientist/Senior Research Scientist in Telcordia Technologies' (formerly Bell Communications Research (Bellcore)) Optical Networking Research Group. His research interests are in optical/telecommunication networks, intelligent transportation networks, IoT, and critical infrastructure systems.